From simulation to experiment: A Sagnac interference-based double holes optical fiber sensor for ultrasensitive Cu(II) detection

Qiang Chen [a,b], Yi Cai [a,b,*] iD, Tianyu Jiang [a], Qing Chen [c,**], Jianhua Wang [d], Yong Zhao [a,b]

[a] School of Control Engineering, Hebei key Laboratory of Micro-Nano Precision Optical Sensing and Measurement Technology, Northeastern University at Qinhuangdao, Qinhuangdao 066004, China
[b] College of Information Science and Engineering, Northeastern University, Shenyang 110819, China
[c] School of Pharmacy, Liaoning Province Key Laboratory for Phenomics of Human Ethnic Specificity and Critical Illness (LPKL-PHESCI), Shenyang Medical College, Shenyang 110034, China
[d] Research Center for Analytical Sciences, Department of Chemistry, College of Sciences, Northeastern University, Shenyang 110819, China

ARTICLE INFO

ABSTRACT

Double-hole optical fiber (DHF) exhibits considerable potential for sensing applications due to its distinctive structural characteristics. In this study, a Sagnac interference (SI) optical fiber sensor based on a corroded DHF shows high refractive index (RI) sensitivity, allowing for the detection of copper ions, Cu(II), at very low concentrations. The dependence of DHF corrosion on the birefringence and RI sensitivity are investigated by the optical simulation. Experimental results illustrate that the RI sensitivity reaches 3267 nm/RIU within the range of 1.3333–1.3743, exhibiting good linearity. A chitosan derivative (CSD) with ion-imprinted (IIM) treatment is coated on the surface of the corroded DHF for Cu(II) detection. It is demonstrated that within the concentration range of Cu(II) from 10^{-15} to 10^{-6} M, both the maximum and average sensitivities can reach 12.08×10^9 and 129.96 nm/μM, respectively, without interference from other metal ions or temperature (25.3–44.0 ℃). The proposed corroded DHF sensor is a good candidate for RI and Cu(II) concentration detection due to its simple structure, high sensitivity, and selectivity.

1. Introduction

The accurate and sensitive detection of refractive index (RI) in the ambient environment holds great significance for chemical and biological applications[1,2]. Compared to traditional semiconductor sensors, optical fiber sensors are advanced due to their small size, low cost, superior performance, remote sensing capabilities, and immunity to electromagnetic interference[3]. A number of researches were carried out on surface plasma resonance (SPR) sensors and optical fiber interference sensors[4] for the detection of RI and other analytes[5]. The operation of optical fiber SPR sensors requires the surface coating of metal film to excite the surface plasmon polaritons, resulting in the use of noble metal materials and high prices. Moreover, the oxidation or damage to the noble metal films has a direct impact on the performance of sensors. Compared to the optical fiber SPR sensors, optical fiber

interference sensors offer the advantages of cost-effectiveness and a long service life. Optical fiber interference sensors typically rely on the phase difference shift. With the assistance of the evanescent field, variations in the ambient environment, such as temperature and RI, can induce a shift in the phase difference, leading to a displacement of interference dips. Relevant research has demonstrated that reducing the distance between the fiber core and its surrounding medium can effectively amplify the evanescent field. Several microstructures were fabricated on the optical fiber, including tapered fiber[6], D-shape fiber[7], etched fiber Bragg gratings[8], and in-line interferometers[9]. However, the fabrication of these microstructures requires the use of sophisticated equipment, such as femtosecond laser ablation and optical fiber grinding platforms. This presents a challenge to the processing of the structures in question. Therefore, further research is imperative to explore the potential of an optical fiber RI sensor with a simple structure and exceptional

* Corresponding author at: School of Control Engineering, Hebei key Laboratory of Micro-Nano Precision Optical Sensing and Measurement Technology, Northeastern University at Qinhuangdao, Qinhuangdao 066004, China.
** Corresponding author.
E-mail addresses: 2310266@stu.neu.edu.cn (Q. Chen), caiyi@qhd.neu.edu.cn (Y. Cai), 2272252@stu.neu.edu.cn (T. Jiang), chenqing0906@symc.edu.cn (Q. Chen), jianhuajrz@mail.neu.edu.cn (J. Wang), zhaoyong@ise.neu.edu.cn (Y. Zhao).
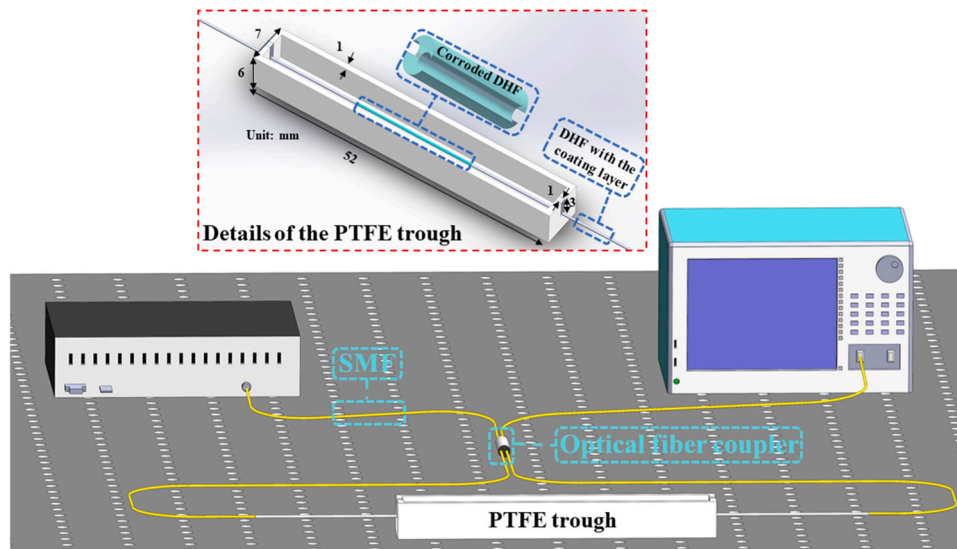
Fig. 1. The schematic diagram of the experimental set-up.

performance.

Recently, optical fiber Sagnac interference (SI) sensors have undergone extensive investigation, with a particular focus on their high sensitivities and consistent performances[10,11]. Optical fiber SI sensors can be employed for measurement of temperature, RI, and strain [12–14]. With special structures and the chemical or physical treatments, the specific parameters can be obtained by the optical fiber SI sensors. Double-hole optical fiber (DHF) is a specialized type of optical fiber that has two holes located on the sides of its core. The short distance between the side holes and the fiber core facilitates a straightforward enhancement of the interaction between the evanescent field and matter. With different durations of corrosion using hydrofluoric acid, the cladding on the exterior of the side holes can be eroded to different degrees. Consequently, DHF is a high-quality optical fiber used in the fabrication of optical fiber SI sensors due to its simple structure, easy fabrication, and superior sensitivity. A good number of studies have been conducted on the corroded-DHF RI measurement in recent years [15,16].

The advancement of industrial production has resulted in the discharge of a considerable quantity of deleterious metal ions, which have led to the contamination of drinking water and posed a significant risk to human health. Copper ions, Cu(II), are among the most pervasive and ubiquitous contaminants. Excessive intake of Cu(II) has been associated with central nervous system damage and the onset of neurodegenerative disorders[17], such as Wilson's disease and Alzheimer's disease. According to the stipulations set forth by the World Health Organization (WHO) and the United States Environmental Protection Agency (US EPA), the maximum permissible concentrations of Cu(II) in potable water are 1.5 and 1.3 ppm, respectively[18]. The detection of Cu (II) with high sensitivity and specificity is therefore of great significance. As the field of chemistry has evolved, several materials have been identified as possessing chelating properties towards heavy metal ions. These include nanoparticles[19], chitosan (CS)[20–22] and DNA[23]. Among these materials, CS is particularly noteworthy for its high content of hydroxyl and amino groups, which confer upon it the ability to adsorb heavy metal ions with great efficiency. However, it lacks selectivity. Several methods have been employed to investigate selectivity, such as, the synthesis of CS derivatives (CSD), the development of ion-imprinted (IIM) CS[24,25] and so on. IIM is a process in which a target metal ion is introduced as a template in a material. Functional monomers are polymerized around the target ion to form cavities that match its shape, size, and chemical environment. Upon removal of the template ions, the cavities exhibit a highly specific recognition of the target ions, thereby significantly enhancing the adsorption selectivity. Several works illustrate that IIM treatment can enhance the selective adsorption of CSD[26].

In this work, an optical fiber SI-based DHF sensor is proposed for the detection of RI and Cu(II) concentration. The impact of the geometrical parameters of the corroded DHF on the performance of the sensor, including the ellipticity of side holes, the ellipticity of the fiber core, the radius of side holes, and the distance between the side holes and the fiber core, has been investigated using optical simulation. It turns out that the sensor exhibits high RI sensitivity, showing a satisfactory correlation between the simulation and experimental results in terms of birefringence and sensitivity parameters. Furthermore, a CSD was synthesized and attached to the surface of the corroded DHF through the hydrogen bond formation. The IIM treatment was conducted on the surface of the corroded DHF, and the concentration of Cu(II) was detected subsequently. The sensor with high RI sensitivity can become a good candidate for low concentration Cu(II) detection due to its high sensitivity, selectivity, and temperature non-crosstalk.

2. Detection mechanism and experimental set-up

2.1. Detection mechanism

The fundamental principle of the optical fiber sensor is SI. Electromagnetic waves transmitted in an optical fiber can be decomposed into mutually orthogonal X-polarization mode (X-PM) and Y-polarization mode (Y-PM). The disparate distribution of RI in the X and Y directions of polarization-maintaining optical fiber (PMF) results in a discrepancy in mode effective RI between X-PM and Y-PM. The construction of an optical fiber Sagnac interferometer loop is facilitated by the utilization of an optical fiber coupler. The transmission intensity of an optical SI Sagnac interferometer loop can be mathematically expressed as[27,28]:

$$T = 10 \times \lg[0.5 \times (1 - \cos(\frac{2\pi}{\lambda} \times B(n) \times L))], B(n) = n_x - n_y, \qquad (1)$$

where T is the transmission intensity of an optical fiber SI loop, B is the birefringence of PMF, n_x and n_y are the effective RI of X-PM and Y-PM fundamental mode, respectively. The symbols λ and L represent the wavelength of the incident wave and the length of PMF, respectively, measured in meters. Lastly, the symbol n refers to the RI of the surroundings.

In this work, the corroded DHF can obtain the information of the surroundings easily. The changes in the RI of the surrounding medium
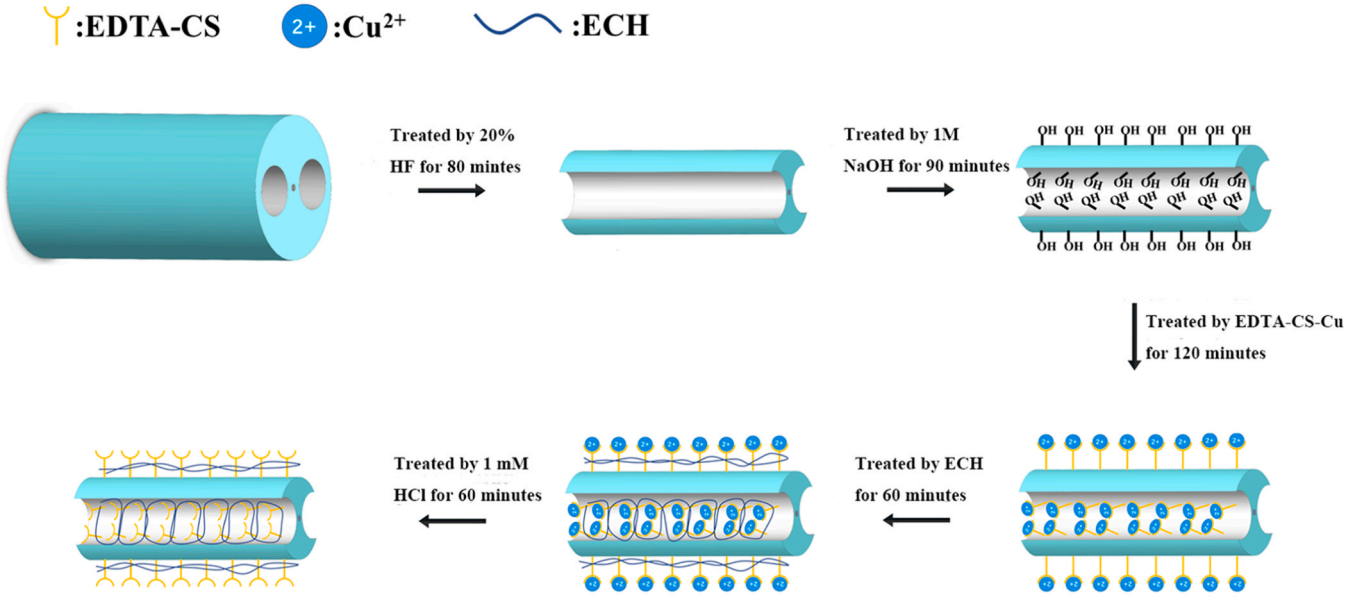
Fig. 2. The schematic diagram of the fabrication process of the sensor.

would significantly affect the birefringence. According to Eq. (1), the wavelength of interference dips could be calculated as:

$$\lambda_m = [B(\lambda, n) \cdot L]/m, \, m = 1, 2, 3..., \tag{2}$$

where λ_m is the wavelength of the mth interference dips. The variation of the surroundings' RI, as demonstrated in Eq. (2), can induce changes in birefringence, consequently leading to shifts in the wavelength of dips. By differentiating Eq. (2) to n, we can get:

$$\left[\left[L \cdot \left(\frac{\partial B(\lambda, n)/\partial \lambda}{\partial \lambda} \cdot \frac{\partial \lambda}{\partial n} + \frac{\partial B(\lambda, n)}{\partial n}\right) + B(\lambda, n) \cdot \frac{\partial L}{\partial n}\right] \cdot \lambda - B(\lambda, n) \cdot L \cdot \frac{\partial \lambda}{\partial n}\right] / \lambda^2 = 0, \tag{3}$$

where $\partial\lambda/\partial n$ is the sensitivity of the sensor, and $\partial L/\partial n = 0$. Through transforming Eq. (3), the sensitivity expression could be obtained as follows:

$$\frac{\partial \lambda}{\partial n} = \lambda \cdot \frac{\partial B(\lambda, n)}{\partial n} \bigg/ \left[B(\lambda, n) - \lambda \cdot \frac{\partial B(\lambda, n)}{\partial \lambda}\right], \tag{4}$$

where $B(\lambda,n)-\lambda \bullet \partial B(\lambda,n)/\partial \lambda$ is defined as the group birefringence. It can be inferred from Eq. (4) that the sensitivity is contingent upon the value of the group birefringence.

2.2. Experimental set-up and procedures

The experimental set-up for RI and Cu(II) concentration detection is depicted in Fig. 1. A supercontinuum light source, with a spectral width of 900–1700 nm, is employed as the light source. The output light is obtained by a Yokogawa optical spectrum analyzer with a resolution of 0.02 nm. A 3 dB optical fiber coupler is employed to construct an optical fiber SI loop, which is then connected to a 15 cm DHF (Yangtze Optical Electronic Co., Ltd, Wuhan, Fiber model:CM00071A11A1T) with a corroded length of 2 cm. The corroded DHF is fixed in a PTFE cell, and the details of this cell are illustrated in Fig. 1. The cell provides an area for the fiber treatment.

The sucrose solutions were diluted to different concentrations in order to achieve various refractive indices for the measurement of the bare corroded DHF sensor. The neutral Cu(II) standard solution (1 g /L, 15.625 mM) with pH value of 7.0 was obtained from National Center for Standard Materials (China) and diluted with DI water. Experimental data were recorded after the spectra were stable. Fig. 2 shows the schematic diagram of the sensor fabrication process.

2.3. Materials

Chitosan (CS) (BR, 80~95 % deacetylation), NaOH, 40 % HF, and $CuSO_4 \cdot 5 \, H_2O$ were bought from Sinopharm Chemical Reagent Co., Ltd.
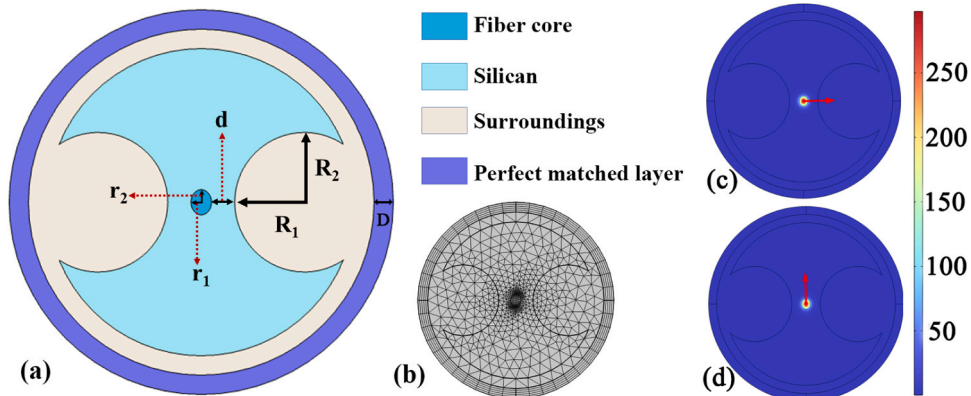

Fig. 3. (a) Simulated corroded DHF structure; (b) Meshed simulated structure; (c) X-PM and (d) Y-PM fundamental modes of electric field.
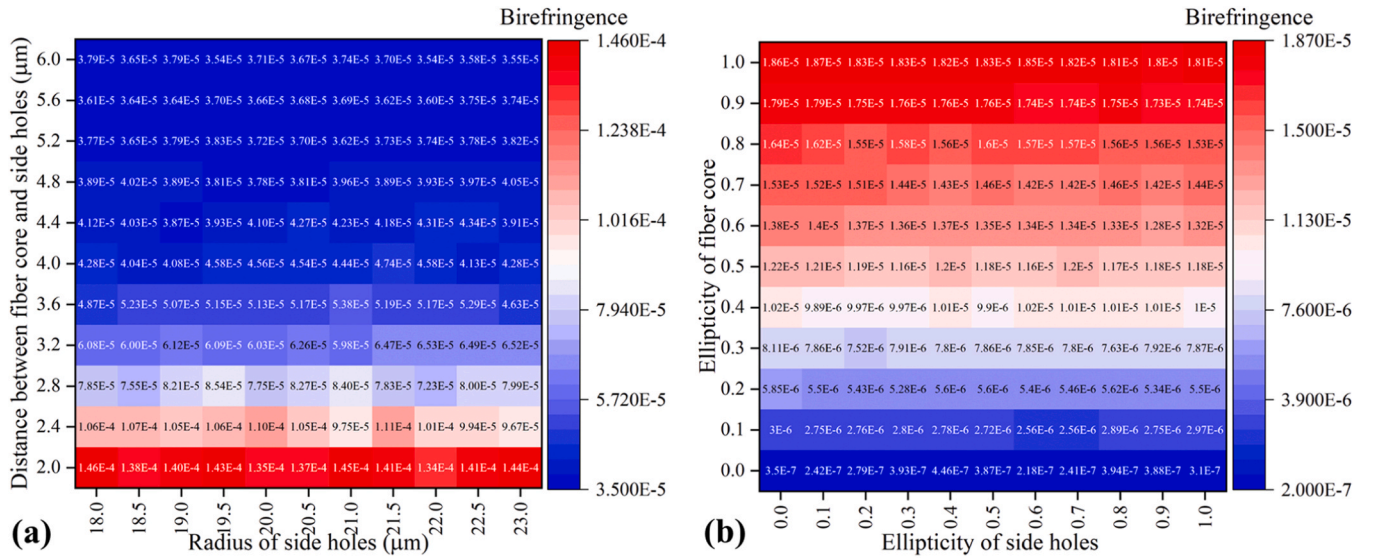
Fig. 4. (a) Dependence of birefringence on the distance and the radius of side holes; (b) Dependence of birefringence on the ellipticity of the fiber core and the side holes.

(Shanghai, China). Ethylenediaminetetraacetic acid (EDTA), 1-ethyl-3-(3-dimethylaminopropyl) carbodiimide hydrochloride (EDAC), N-Hydroxysuccinimide (NHS), disodium phosphate, epichlorohydrin (ECH) were obtained from Aladdin Chemical Co., Ltd. (Shanghai, China). Deionized water (DI water) with a pH of 7.0 and resistivity of 18.2 MΩ·cm was used through experiment. The details of the CSD synthesis and fabrication process of the sensor are described in the Supplementary Materials.

3. Results and discussions

3.1. The results of optical simulation

Simulation optimizations have been conducted using the COMSOL Multiphysics software, which employs the finite element method. The configuration of the simulation structure is illustrated in Fig. 3(a). The semi-short and semi-long axes of the fiber core are designated as r_1 and

r_2, respectively. The semi-short and semi-long axes of side holes are designated R_1 and R_2, respectively. The distance between the side holes and fiber core is denoted as d, while the thickness of the perfect matched layer (PML) is defined as $D = 10$ μm. The PML is defined at the surface of the surrounding domain, and a scattering boundary condition is introduced at the PML boundary. The meshed structure of the model is illustrated in Fig. 3(b). The meshed structure consists of 1134 domain elements and 136 boundary elements, with a minimum element size of 0.039 μm and a maximum element size of 8.71 μm. The results of the simulations for the optical electric field of the X-PM and Y-PM fundamental modes in optical fiber are presented in Fig. 3(c) and (d), respectively. The effective RI of the X-PM and Y-PM fundamental modes are obtained at different surrounding refractive indices while scanning wavelengths of 900–1700 nm with a step size of 1 nm.

The background material of DHF is silica, and the RI of silica could be described by the Sellmeier equation[29]:
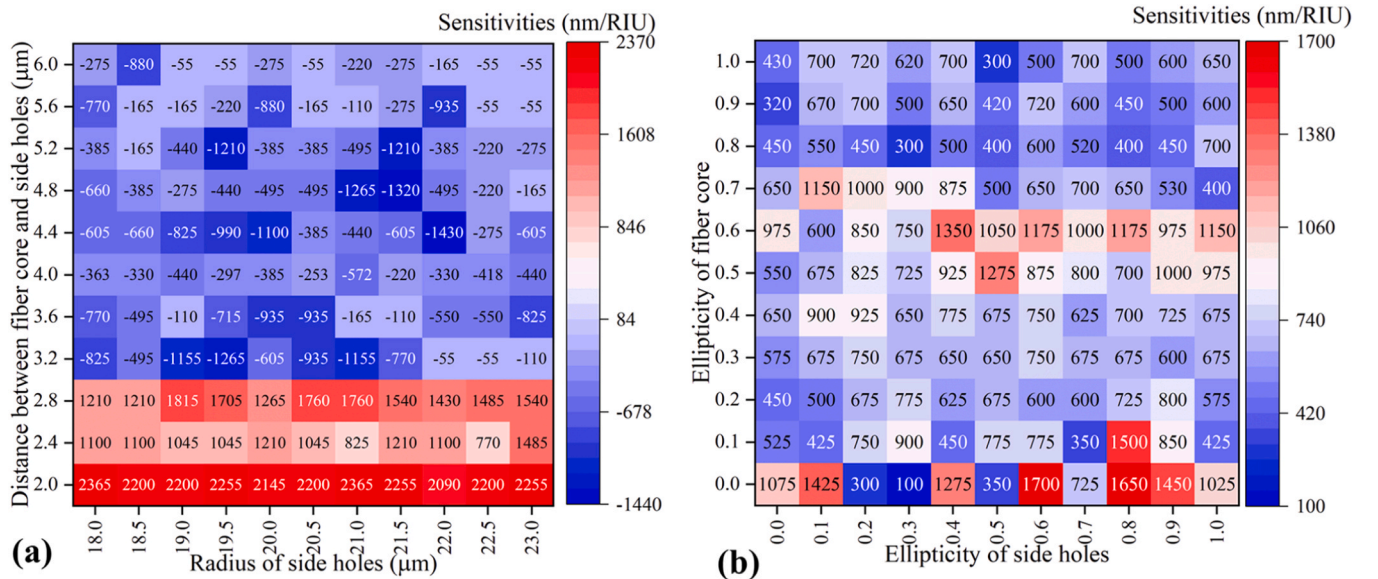

Fig. 5. (a) The dependence of sensitivities on the distance and the radius of side holes; (b) The dependence of sensitivities on the ellipticity of the fiber core and the side holes.

$$n_{Si}^2 = 1.31552 + 6.90754$$

$$\times 10^{-6}t + \frac{(0.788404 + 2.35835 \times 10^{-5}t)\lambda^2}{\lambda^2 - (0.0110199 + 0.584758 \times 10^{-6}t)}$$

$$+ \frac{(0.91316 + 0.548368 \times 10^{-6}t)\lambda^2}{\lambda^2 - 100}, \tag{5}$$

where n_{Si}^2 represents the RI of silica, and t is the temperature. The temperature was set at 30 ℃. The thermo-optic coefficient of silica is low (around -4.2×10^{-6} RIU/℃), thus the temperature has little influence on the simulation results. The RI of the core is set to be 0.01 higher than that of silica.

A simulation was conducted to investigate the influence of four parameters (radius of side holes, distance between the side holes and the fiber core, ellipticity of fiber core, ellipticity of side holes) on the maximum birefringence and average sensitivity of this sensor. The radius of the side holes was increased from 18 μm to 23 μm in increments of 0.5 μm, while the distance between the side holes and the fiber core was increased from 2 μm to 6.0 μm in increments of 0.4 μm. The ellipticity of the side holes and the fiber core ranged from 0 to 1 with increments of 0.1, while the semi-short axis of the fiber core was set at 2.5 μm and that of the side holes was set at 18 μm. The average sensitivity and maximum birefringence were calculated for all cases in which the surrounding RI increased from 1.33 to 1.37 within the wavelength range of 0.9–1.7 μm. The results of the simulation are presented in Fig. 4 and Fig. 5.

Fig. 4(a) and (b) demonstrate that the birefringence of the sensor is significantly influenced by the distance between the fiber core and side holes, as well as the ellipticity of the fiber core. The radius and ellipticity of the side holes are found to have little impact on birefringence. As the distance between the side holes and fiber core increases from 2 to 6 μm, the birefringence decreases from approximately 1.46×10^{-4} to 3.79×10^{-5}. In contrast, the birefringence remains relatively constant as the radius of side holes increases. As the ellipticity of the fiber core increases from 0 to 1.0, the birefringence increases from approximately 3.5×10^{-7} to 1.86×10^{-5}. However, the variations in the ellipticity of the side holes have a negligible impact on the birefringence. The simulation results on birefringence illustrate that, once the ellipticity of the fiber core is established, the radius of the side holes can be increased through hydrofluoric acid corrosion, thereby reducing the distance between the side holes and the fiber core. This process serves to increase the birefringence of the sensor.

Fig. 5(a) and (b) demonstrate how these four parameters affect the sensitivity of the sensor. It is also observed that the birefringence exhibits a corresponding variation in response to the alterations in the aforementioned parameters, thereby exerting an influence on the calculated sensitivity. As illustrated in Fig. 5(a), the sensitivity of this sensor undergoes a transition from positive to negative as the distance between the side holes and the fiber core exceeds 2.8 μm. The primary reason for this phenomenon is the alteration of group birefringence to a negative state when the distance between the side holes and the fiber core exceeds 2.8 μm. Furthermore, the absolute value of sensitivity decreases with the increasing distance between the side holes and the fiber core. The maximum sensitivity reaches 2365 nm/RIU when the distance between the side holes and the fiber core is 2 μm and the radius of the side holes is 18 μm. The irregular and disorganized impact of the radius of the side holes on sensitivity is also a notable phenomenon. As illustrated in Fig. 5(b), the sensitivity remains positive when the ellipticity of the fiber core and the side holes are varied from 0 to 1. However, the impacts of the ellipticity of the fiber core and the side holes on the sensitivity are also irregular and disorganized. The ellipticity of the fiber core and the side holes is difficult to change once the optical fiber is fabricated, while the distance between the fiber core and side holes can be changed through chemical corrosion. A conclusion can be drawn that, once the ellipticity of the fiber core and the side holes has been established, the distance between the side holes and the fiber core of DHF
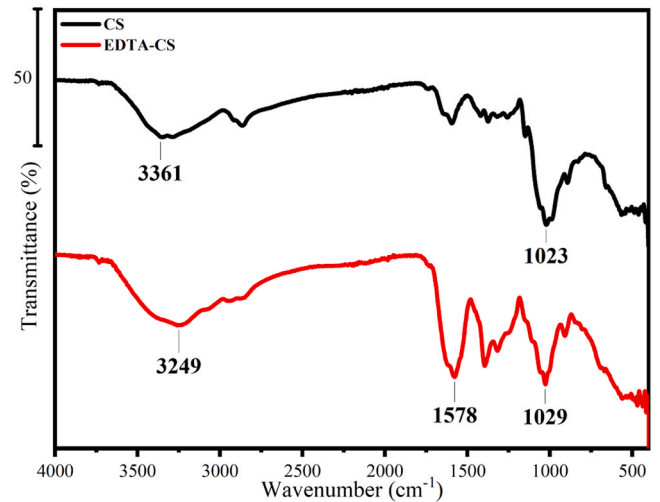

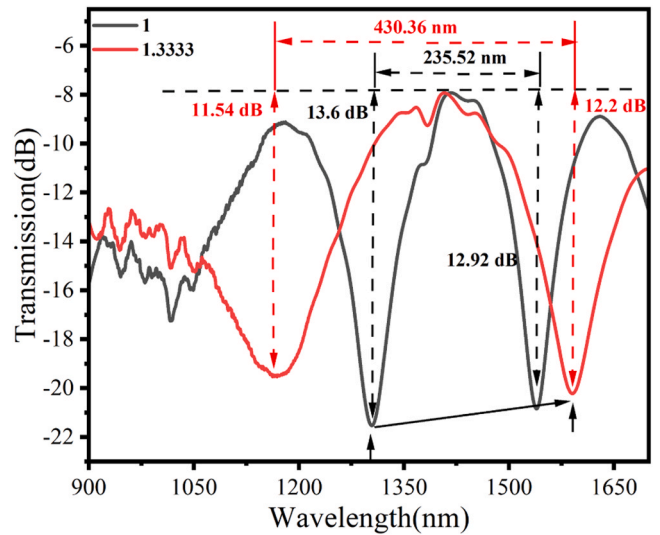Fig. 6. FTIR analysis of the CS and EDTA-CS.

Fig. 7. The transmission spectra of corroded DHF in ambient air and DI water.

could be decreased through HF corrosion, thereby increasing sensitivity.

3.2. The characteristics of the Cu(II)-sensitive material

FTIR analysis of CS and EDTA-CS revealed functional groups in the materials, as illustrated in Fig. 6. Compared between the FTIR curves of CS and EDTA-CS, the appearance of the peak at 1578 cm^{-1} of EDTA-CS corresponds to the stretching vibration absorption of unsaturated double bonds C=O or C=N. The synthesis of EDTA-CS contributes to the introduction of carboxyl groups, thereby enhancing the chelating capacity for Cu(II).

3.3. RI test

The detection performances of this bare corroded DHF are investigated for RI, and the results are presented in Fig. 7. The transmission spectrum shows two interference dips, as shown in Fig. 7, with extinction ratios of approximately 14 dB and a free spectral range of 235.52 nm when the bare corroded DHF is placed in the air. Upon immersion of the bare corroded DHF in DI water, both interference dips exhibit a shift towards longer wavelengths. The extinction ratios vary to approximately 12 dB and the free spectral range expands to 430.36 nm.
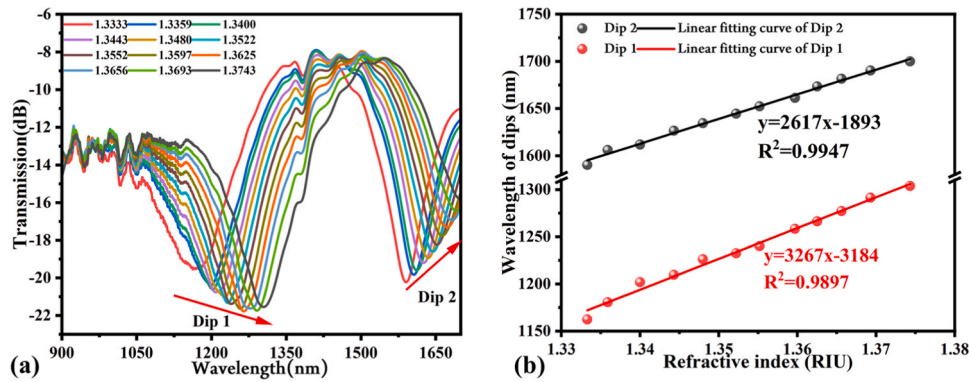
Fig. 8. (a) The transmission spectra of corroded DHF in solutions with different RI; (b) The corresponding fitting curves of Dip1 and Dip 2, respectively.

Table 1
Comparison of the sensitivities of this work with those of previous works.

Sensor structures	Maximum sensitivities (nm/RIU)	Detection principles	References
U-bend single mode fiber in optical free quency domain reflectometry	39.08	Multimodel interference	[30]
Gold film-coated tapered single-mode fiber	2021.07	MZI	[31]
Double-Peanut and Er-Doped Fiber Taper Structure	441.56	MZI	[32]
Gold coated photonic crystal fiber sandwiched by two collapsed multimode fiber	1947.405	SPR in Mach-Zehnder interference (MZI)	[33]
Corroded DHF	3266.76	SI	This work

From Eq. (2), the birefringence of a SI sensor can be calculated as follows:

$$B = \lambda_m \cdot \lambda_{m+1} / [(\lambda_{m+1} - \lambda_m) \cdot L], \tag{6}$$

Upon immersion in water, the bare sensor exhibits two dips at 1162.44 nm and 1591.34 nm, which are labeled as Dip 1 and Dip 2, respectively. The length of this sensor is approximately 3 cm. According to Eq. (6), the birefringence can be calculated as 1.433×10^{-4}. The simulation results demonstrate that when the distance between the fiber core and side holes is 2 μm, and the radius of the side holes is 23 μm, the simulated birefringence approximates 1.44×10^{-4}. This indicates that the experimental and simulation results are in good agreement.

As illustrated in Fig. 8(a), both dips exhibit a redshift as the RI increased from 1.3333 to 1.3743. As illustrated in Fig. 8(b), the fitting equations of Dip 1 and Dip 2 are y = 3267x-3184 and y = 2617x-1893, with R^2 of 0.9897 and 0.9947, respectively. The RI sensitivities of Dip 1 and Dip 2 are 3267 and 2167 nm/RIU, respectively.

The limit of detection (LOD) for the linearity response sensor is defined as $LOD_{RI} = \alpha/S$, where LOD_{RI} represents the LOD for RI detection, α denotes the resolution of the detector and S stands for the sensitivity of the sensor. The resolution of the detector in this experiment was set to 0.02 nm. The LODs are thus concluded to be 6 μRIU for Dip 1 and 8 μRIU for Dip 2, respectively.

The comparison of the sensitivities of this work with those of previous research is shown in Table 1. The proposed method, with its simple structure, shows higher sensitivity compared to other researches (ref. [30–33]), making it a promising candidate for the RI measurement.

3.4. Cu(II) concentration detection

Before the detection, the sensor should be calibrated. The sensor is immersed in DI water with a pH of 7.0 until the spectrum became stable. The spectrum is considered to be the spectrum when no Cu(II) are present. As illustrated in Fig. 9(a), when the corroded DHF is coated with an EDTA-CS-ECH film, only a single interference dip is observed in the transmission spectrum, with an extinction ratio of approximately 15 dB. The transmission spectra obtained from the sensor with different Cu(II) concentrations are illustrated in Fig. 9(b). The interference dip shifts towards longer wavelengths. The extinction ratio decreases as the Cu(II) concentration increases from 10^{-15} M to 10^{-6} M. This phenomenon can be attributed to the EDTA-CS attached to the surface of the corroded DHF, which can chelate Cu(II). This process contributes to an increased RI around the sensor, resulting in a redshift of the SI dip. Fig. S4 illustrates the wavelength shift value changes with the immersion time when the Cu(II) concentration is 10^{-9} M. After 10 minutes, the transmission
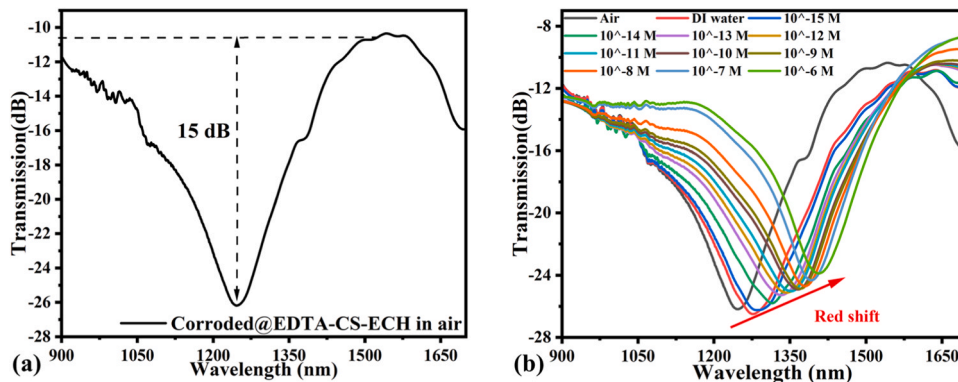

Fig. 9. (a) Transmission spectrum of corroded DHF coating by EDTA-CS-ECH in the air; (b) Transmission spectra of corroded DHF coating by EDTA-CS-ECH in Cu(II) solutions with different concentrations.
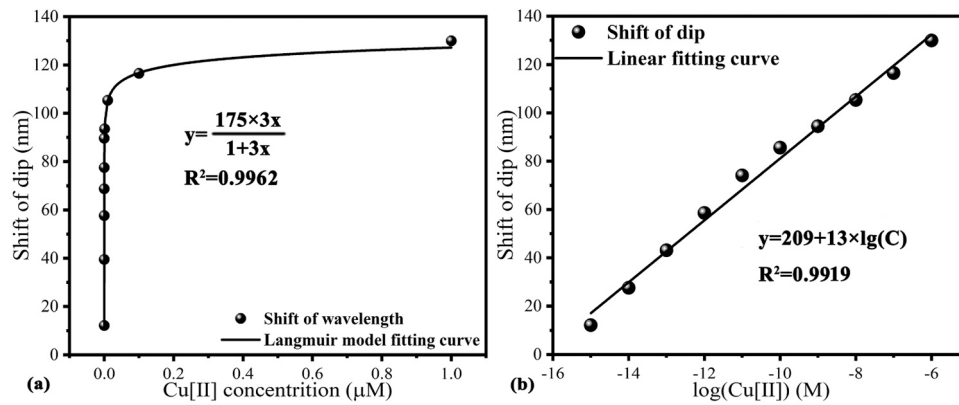
Fig. 10. (a) The obtained fitting curve between the shift of dip and the Cu(II) concentration with the Langmuir isotherm model; (b) The corresponding fitting curve between the shift of dip and logarithm of the Cu(II) concentration.
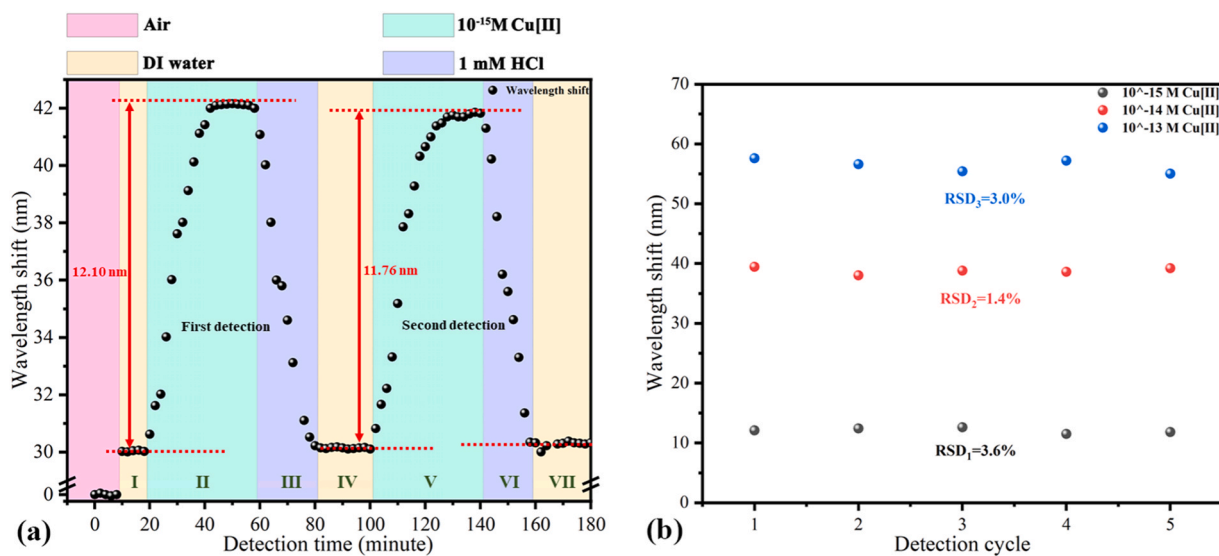

Fig. 11. (a) The test result of reusability of the sensor; (b) The test result of repeatability of the sensor.

spectrum became stable.

The LOD was determined by utilizing the Langmuir isotherm model, which is expressed as follows[34]:

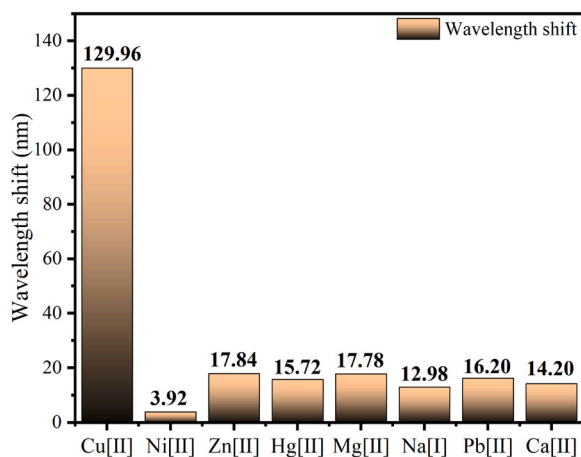$$\Delta\lambda = \Delta\lambda_{max} \cdot K \cdot C / (1 + K \cdot C),$$

Fig. 12. Wavelength shift when the sensor immersed in 1 μM metal ions solutions, respectively.

where $\Delta\lambda$ represents the wavelength shift, $\Delta\lambda_{max}$ denotes the maximum wavelength shift when the film is saturated with adsorbed Cu(II), and K represents the equilibrium binding constant under steady-state conditions. The fitting curve based on the Langmuir model, which is shown in Fig. 10(a), illustrates a good fit. The $\Delta\lambda_{max}$ and K values of the Langmuir isotherm model are 175 nm and 3, respectively. Moreover, the fabricated sensor exhibited a higher sensitivity towards lower Cu(II) concentrations, while the sensitivity gradually decreased as the concentration of Cu(II) increased. In the concentration range of $10^{-9}\sim1$ μM, the maximum sensitivity is 12.08×10^9 nm/μM, and the average sensitivity is 129.96 nm/μM. The fitting equation is depicted in Fig. 10(b), demonstrating a strong linear fit with an R^2 value of 0.9919. The shift of the SI dip is approximately 12.81 nm when the concentration of Cu(II) increases tenfold.

For the Langmuir isotherm model response sensor, the LOD is defined as follows[35]:

$$LOD_{Cu(II)} = \alpha / [K \cdot (\Delta\lambda_{max} - \alpha)],$$

where $LOD_{Cu(II)}$ represents the LOD for the Cu(II) detection, α denotes the resolution of the detector, and K and $\Delta\lambda_{max}$ are the parameters of the fitting function. In this experiment, the detector resolution was set to 0.02 nm. The LOD of this sensor is calculated as 4.27×10^{-5} μM.

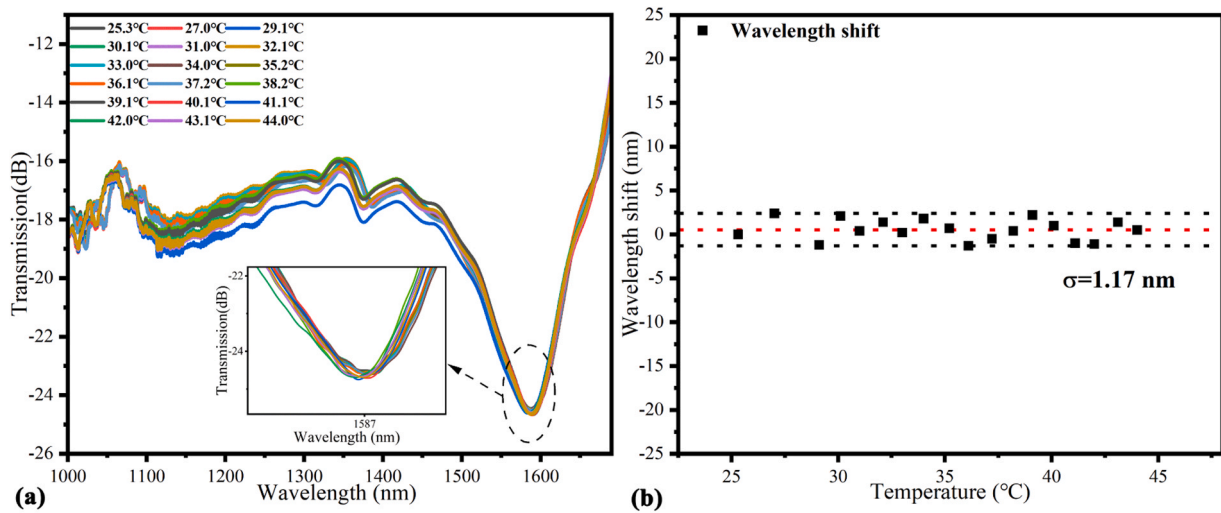The reusability and repeatability of this sensor are tested. The result

Fig. 13. (a) Transmission spectra obtained from the sensor at different temperatures; (b) The dependence of wavelength shifts on temperature.

Table 2

Comparison of the sensor structure, functional materials, concentration range, LOD$_{Cu(II)}$, and sensitivity of this work with those of previous works.

Sensor structure	Functional materials	Concentration range	LOD$_{Cu(II)}$	Sensitivity	reference
Single mode fiber-photonic crystal fiber-single mode fiber structure for MZI excitation	CS crosslinked by epichlorohydrin	5 μM–1 mM	0.57 μM	0.0632 nm/μM	[37]
Tapered multimode fiber for MZI excitation	Polydopaminemaleic acid	10^{-14}–10^{-6} M	8×10^{-6} μM	185 nm/μM	[36]
Multimode fiber with a core diameter of 600 μm coated with gold film for SPR excitation	Graphene oxide and Ni^{2+}-imprinted chitosan	5 μM–1.7 mM	4×10^{-2} μM	5.22 nm/[lg(mg/L)]	[38]
Corroded double holes fiber for Sagnac interference excitation	Chitosan derivative with ion-imprinted	10^{-15}–10^{-6} M	4.27×10^{-5} μM	129.96 nm/μM	This work

is shown in Fig. 11. As shown in Fig. 11(a), when the sensor is immersed in the solution containing 10^{-15} M Cu(II), the wavelength shift is 12.10 nm. Before the second detection, the sensor is treated with 1 mM HCl for 20 minutes. The maximum wavelength shift in the second detection is 11.76 nm, which shows a slight difference (0.34 nm) compared to that of the first detection. As shown in Fig. 11(b), the relative standard deviations (RSD) are 3.6 %, 1.4 %, and 3.0 % when the Cu(II) concentration is 10^{-15}, 10^{-14}, and 10^{-13} M respectively, illustrating the detection results are accuracy and the sensor is repeatable.

3.5. Interferences

The selective detection of metal ions is a crucial aspect for the proposed sensor. In this study, the interferences of other metal ions of the optical fiber sensor were investigated. It is shown in Fig. 12 that the spectrum exhibits a slight redshift when 1 μM of Ni(II), Zn(II), Hg(II), Mg(II), Na(I), Pb(II), and Ca(II) are added to the solution. The spectra in Fig. 12 demonstrate that, the dip shifts are 129.96, 3.92, 17.84, 15.72, 17.78, 12.98, 16.20, and 14.20 nm for the 1 μM Cu(II), Ni(II), Zn(II), Hg (II), Mg(II), Na(I), Pb(II), and Ca(II) solutions, respectively. The maximum selective factor reaches 33. The CSD film can chelate other metal ions, while the Cu(II) IIM treatment of the CSD film enhances the Cu(II) complexation ability of CSD.

Optical fiber based on SI is typically vulnerable to temperature-related fluctuations due to the photothermal effect of PMF. The dependence of wavelength shifts on temperature is investigated. The experimental set-up for the temperature test is illustrated in Fig. S5. As shown in Fig. 13(a), the spectra exhibit no obvious change as the temperature increases from 25.3 ℃ to 44.0 ℃. The maximum wavelength shift is 2.4 nm. The mean and standard deviation values of floating is 0.52 nm and σ= 1.17 nm, respectively, illustrating that temperature has little influence on the sensor. The temperature-insensitive property

undoubtedly benefits the detection of RI and Cu(II). The DHF lacks stress rods, which makes the sensor less sensitive to temperature variations.

The comparison of the sensor structure, functional material, concentration range, LOD, and sensitivity of this work with those of previous research is shown in Table 2. Compared with other works from ref [36–38], this designed sensor has the advantages of high sensitivity, low LOD, and simple structure, making it a good candidate for Cu(II) detection.

4. Conclusion

In this study, a sensitive corroded DHF sensor was designed based on SI. Optical simulation illustrated that the corrosion of DHF can enlarge the birefringence and RI sensitivity. Experimental results illustrated that the maximum RI sensitivity reached 3266.76 nm/RIU with good linearity, and the birefringence reached 1.433×10^{-4}. The EDTA-CS film with IIM treatment was coated on the corroded DHF for the selective and sensitive detection of Cu(II). Experimental results showed that the average sensitivity for Cu(II) detection reached 129.96 nm/μM in the range of 10^{-15}~10^{-6} M without the interference of other metal ions. There is also no temperature crosstalk in the range of 25.3–44.0 ℃. The proposed sensor showed excellent performance through the simulation to experiment.

CRediT authorship contribution statement

Cai Yi: Writing – review & editing. **Chen Qing:** Writing – review & editing. **Jiang Tianyu:** Writing – review & editing. **Zhao Yong:** Writing – original draft, Funding acquisition. **Wang Jianhua:** Writing – review & editing. **Chen Qiang:** Writing – original draft.

Declaration of Competing Interest

The authors declare no competing financial interest.

Acknowledgments

Appendix A. Supporting information

Supplementary data associated with this article can be found in the online version at doi:10.1016/j.snb.2025.137692.

Data availability

Data will be made available on request.

References

[1] Y. Zhao, X. Hu, S. Hu, Y. Peng, Applications of fiber-optic biochemical sensor in microfluidic chips: a review, Biosens. Bioelectron. 166 (2020) 112447.

[2] Y. Zhou, Y. Zhang, B. Han, L. Cheng, D. Li, W. Zheng, Y. Zhao, Biochemical sensor based on functional material assisted optical fiber surface plasmon resonance: a review, Measurement 207 (2023) 112353.

[3] M. Elsherif, A.E. Salih, M.G. Muñoz, F. Alam, B. AlQattan, D.S. Antonysamy, M. F. Zaki, A.K. Yetisen, S. Park, T.D. Wilkinson, H. Butt, Optical fiber sensors: working principle, applications, and limitations, Adv. Photon. Res. 3 (2022) 2100371.

[4] Y. Liu, W. Peng, Fiber-optic surface plasmon resonance sensors and biochemical applications: a review, J. Light. Technol. 39 (2021) 3781–3791.

[5] S. Soares, A. Giannetti, F. Esposito, L. Sansone, A. Srivastava, S. Campopiano, M. Giordano, M. Facão, N.F. Santos, A. Iadicicco, C. Marques, F. Chiavaioli, Cortisol detection using a long period fiber grating immunosensor coated with graphene oxide, Sens. Actuators Rep. 9 (2025) 100279.

[6] N. Chen, X. Zhou, X. Li, Highly sensitive humidity sensor with low-temperature cross-sensitivity based on a polyvinyl alcohol coating tapered fiber, IEEE Trans. Instrum. Meas. 70 (2021) 9503308.

[7] Y. Wang, B. Liu, Y. Pang, J. Liu, J. Shi, S. Wan, X. He, J. Yuan, Q. Wu, Low-cost wearable sensor based on a D-shaped plastic optical fiber for respiration monitoring, IEEE Trans. Instrum. Meas. 70 (2021) 4004808.

[8] V. Kumar N, K. BS, S. Asokan, Selective detection of lead in water using etched fiber Bragg grating sensor, Sens. Actuators B Chem. 354 (2022) 131208.

[9] Y. Du, S. Jothibasu, Y. Zhuang, C. Zhu, J. Huang, Rayleigh backscattering based macrobending single mode fiber for distributed refractive index sensing, Sens. Actuators B Chem. 248 (2017) 346–350.

[10] Q. Chen, H. Chen, Y. Liu, Z. Gao, B. Wu, X. Fan, C. Liu, H. Li, Y. Li, M. Ma, An optical fiber sensor for the detections of liquid level and strain through cascading Sagnac interference and modal interference, Infrared Phys. Technol. 127 (2022) 104387.

[11] R. Tabassum, B.D. Gupta, Fiber optic manganese ions sensor using SPR and nanocomposite of ZnO–polypyrrole, Sens. Actuators B Chem. 220 (2015) 903–909.

[12] Y. Yang, Y. Zhang, X. Mu, L. Sun, J. Wang, Y. Li, J. Gao, L. Bi, Fiber optic temperature sensor based on the harmonic vernier effect generated by two Sagnac interferometers, IEEE Sens. J. 24 (2024) 12419–12425.

[13] X. Li, S.C. Warren-Smith, H. Ebendorff-Heidepriem, Y. Zhang, L.V. Nguyen, Optical fiber refractive index sensor with low detection limit and large dynamic range using a hybrid fiber interferometer, J. Light. Technol. 37 (2019) 2954–2962.

[14] C. Liu, H. Chen, Q. Chen, Z. Gao, B. Wu, X. Fan, M. Ma, Sagnac interferometer-based optical fiber strain sensor with exceeding free spectral measurement range and high sensitivity, Opt. Laser Technol. 159 (2023) 108935.

[15] T. Liu, H. Zhang, L. Xue, B. Liu, H. Liu, B. Huang, J. Sun, D. Wang, Highly sensitive torsion sensor based on side-hole-fiber Sagnac interferometer, IEEE Sens. J. 19 (2019) 7378–7382.

[16] F. Zhao, W. Lin, J. Hu, S. Liu, F. Yu, X. Chen, G. Wang, P.P. Shum, L. Shao, Salinity and temperature dual-parameter sensor based on fiber ring laser with tapered side-hole fiber embedded in Sagnac interferometer, Sensors 22 (2022) 8533.

[17] Y. Song, K. Qu, C. Xu, J. Ren, X. Qu, Visual and quantitative detection of copper ions using magnetic silica nanoparticles clicked on multiwalled carbon nanotubes, Chem. Commun. 46 (2010) 6572–6574.

[18] T. Roychowdhury, H. Tokunaga, M. Ando, Survey of arsenic and other heavy metals in food composites and drinking water and estimation of dietary intake by the villagers from an arsenic-affected area of west Bengal, India, Sci. Total Environ. 308 (2003) 15–35.

[19] E. Priyadarshini, N. Pradhan, Gold nanoparticles as efficient sensors in colorimetric detection of toxic metal ions: a review, Sens. Actuators B Chem. 238 (2017) 888–902.

[20] M. Zhang, G. Zhu, T. Li, X. Lou, L. Zhu, A dual-channel optical fiber sensor based on surface plasmon resonance for heavy metal ions detection in contaminated water, Opt. Commun. 462 (2020) 124750.

[21] K. Sadani, P. Nag, S. Mukherji, LSPR based optical fiber sensor with chitosan capped gold nanoparticles on BSA for trace detection of Hg(II) in water, soil and food samples, Biosens. Bioelectron. 134 (2019) 90–96.

[22] I. Yulianti, N.M.D. Putra, Fianti, N. Akmalia, D.A. Pratiwi, I.V. Albadiah, Study of chitosan layer-based Fabry Perot interferometer optical fiber sensor properties for detection of Pb^{2+}, Hg^{2+} and Ni^{2+}, J. Phys.: Conf. Ser. 1170 (2019) 012079.

[23] M.R. Saidur, A.R.A. Aziz, W.J. Basirun, Recent advances in DNA-based electrochemical biosensors for heavy metal ion detection: a review, Biosens. Bioelectron. 90 (2017) 125–139.

[24] H. Yan, J. Dai, Z. Yang, H. Yang, R. Cheng, Enhanced and selective adsorption of copper(II) ions on surface carboxymethylated chitosan hydrogel beads, Chem. Eng. J. 174 (2011) 586–594.

[25] L. Zhou, C. Shang, Z. Liu, G. Huang, A.A. Adesina, Selective adsorption of uranium (VI) from aqueous solutions using the ion-imprinted magnetic chitosan resins, J. Colloid Interface Sci. 366 (2012) 165–172.

[26] W. Zhang, M. Yun, Z. Yu, D. Chen, X. Li, A novel Cu(II) ion-imprinted alginate–chitosan complex adsorbent for selective separation of Cu(II) from aqueous solution, Polym. Bull. 76 (2019) 1861–1876.

[27] L. Shao, Y. Luo, Z. Zhang, X. Zou, B. Luo, W. Pan, L. Yan, Sensitivity-enhanced temperature sensor with cascaded fiber optic Sagnac interferometers based on vernier-effect, Opt. Commun. 336 (2015) 73–76.

[28] Y. Zhao, M. Dai, Z. Chen, X. Liu, M.S.A. Gandhi, Q. Li, H.Y. Fu, Ultrasensitive temperature sensor with vernier-effect improved fiber Michelson interferometer, Opt. Express 29 (2021) 1090–1101.

[29] Q. Chen, H. Chen, Y. Liu, Y. Wang, X. Fan, G. Bai, M. Zhang, H. Du, A self-verification temperature sensor based on surface plasmon resonance in a hollow core negative curvature fiber, J. Phys. D: Appl. Phys. 55 (2022) 225208.

[30] P. Xu, X. Yu, Z. Chen, L. Sheng, J. Liu, S. Zhou, K. Wen, O. Xu, X. Dong, J. Yang, Y. Qin, Distributed refractive index sensing based on bending-induced multimodal interference and rayleigh backscattering spectrum, Opt. Express 29 (2021) 21530–21538.

[31] X. Chen, X. Li, D. Yi, X. Hong, Y. Chen, Plasmonic tapered-fiber interference sensor for simultaneously detecting refractive index and temperature, Opt. Lett. 46 (2021) 6071–6074.

[32] F. Zhao, D. Xiao, W. Lin, Y. Chen, G. Wang, J. Hu, S. Liu, F. Yu, W. Xu, X. Yang, L. Yibin, L. Shao, P.P. Shum, W. Wang, Sensitivity enhanced refractive index sensor with in-line fiber Mach-Zehnder interferometer based on double-peanut and er-doped fiber taper structure, J. Light. Technol. 40 (2022) 245–251.

[33] R. Tong, Y. Wang, K. Zhao, Y. Zhao, Surface plasmon resonance optical fiber sensor for refractive index detection without temperature crosstalk, IEEE Trans. Instrum. Meas. 71 (2022) 7002806.

[34] R. Raghunandhan, L.H. Chen, H.Y. Long, L.L. Leam, P.L. So, X. Ning, C.C. Chan, Chitosan/PAA based fiber-optic interferometric sensor for heavy metal ions detection, Sens. Actuators B Chem. 233 (2016) 31–38.

[35] S. Maguis, G. Laffont, P. Ferdinand, B. Carbonnier, K. Kham, T. Mekhalif, M. Millot, Biofunctionalized tilted fiber Bragg gratings for label-free immunosensing, Opt. Express 16 (2008) 19049–19062.

[36] G. Wang, D. Sun, L. Liang, G. Wang, J. Ma, Highly sensitive detection of trace lead ions concentration based on a functional film-enhanced optical microfiber sensor, Opt. Laser Technol. 161 (2023) 109171.

[37] R. Ravikumar, L.H. Chen, M.M. Xin Hui, C.C. Chan, Ion-imprinted chitosan-based interferometric sensor for selective detection of heavy metal ions, J. Light. Technol. 37 (2019) 2778–2783.

[38] Y. Ma, W. Zheng, Y. Zhang, X. Li, Y. Zhao, Optical fiber SPR sensor with surface ion imprinting for highly sensitive and highly selective Ni^{2+} detection, IEEE Trans. Instrum. Meas. 70 (2021) 7006006.

Qiang Chen was born in Cangzhou, Hebei Province, China in 1997. He received his master's degree from Yanshan University in 2023. He is currently pursuing his doctoral degree at the School of Information Science and Engineering, Northeastern University, Shenyang, China. His supervisor is Dr. Cai. His research is focus on the design of optic interference structures of fiber sensor and their application in chemical sensing.

Yi Cai was born in Liaoning Province, China in 1989. She received her Ph.D. degree in Analytical Chemistry (2018) from Northeastern University, China. She is an associate professor in Northeastern University (Qinhuangdao Campus). Her research interests include the development of fiber sensing platforms based on novel fluorescent materials and the development of other miniaturized photoelectric devices for detection.

Tianyu Jiang was born in Zibo, Shandong Province, China in 1997. He received his bachelor's degree from Qufu Normal University in 2020. He is currently pursuing his master's degree at the Northeastern University (Qinhuangdao Campus). His research is focus on the fluorescent fiber sensor and the applications.

Qing Chen received MA and PhD degrees from Northeastern University in 2014 and 2018, respectively. Then, she worked as an associate professor at Shenyang Medical College. Her research interests include the bio-nanomaterials, precision medicine, and proteomics.

Jianhua Wang received the Ph.D. degree in analytical chemistry from the Technical University of Denmark, Lyngby, Denmark, in 2002, with Prof. Elo Harald Hansen as the Supervisor. He joined Northeastern University, Shenyang, China, in 2003, where he is

currently a Professor in analytical chemistry with the Research Center for Analytical Sciences. He has authored or coauthored more than 200 articles. His research interests include flow analysis and sample pretreatment, microfluidic/mesofluidic analytical systems, and applications in life sciences, metallomics, and atomic spectrometry/mass spectrometry. Dr. Wang received a few awards including the FIA Award for Science. He has been an Associate Editor of Talanta since 2004. He is the supervisor of Dr. Cai.

Yong Zhao received MA and PhD degrees, respectively, from Harbin Institute of Technology in 1998 and 2001. Then he worked as a postdoctoral research fellow, an associate professor until 2009 in Tsinghua University. Now he is working at the Northeastern University as a full professor. In 2014, he was awarded by the National Science Foundation for Distinguished Young Scholars of China. In 2015, he was honored as the Yangtze River Scholar Distinguished Professor by the Ministry of Education of China. His current research interests are the development of fiber-optic sensors and device, fiber Bragg grating sensors, novel sensor materials and principles, and optical measurement technologies. He has authored and co-authored more than 300 scientific papers, 60 patents, and 5 books.